15.2. Radar polarimetric signatures of fire plumes

V. Melnikov[(*)], D.S. Zrnic[(#)], R.M. Rabin[(#)], R. B. Pierce[(+)], P. Zhang[(*)]

[(*)] Cooperative Institute for Mesoscale Meteorological Studies, University of Oklahoma, Norman, OK.
[(#)] NOAA/OAR National Severe Storms Laboratory, Norman, OK.
[(+)] NESDIS Atmospheric Research and Applications Division, Madison, WI

1. Introduction

Remote identification of plumes helps to locate wild fires, estimate effectiveness of fire operations, and predict impacts on air quality. A number of remote sensing techniques are used to identify and study wild fire plumes: visible and shortwave infrared observations from satellites, lidar backscatter, and radar observations. Observations at shortwave infrared frequencies from satellite have been effective in monitoring location of fires in cloud free regions. For example, the Automated Biomass Burning Algorithm (ABBA) has been providing maps of fires in South America for more than a decade and is currently being applied in real-time over North America (Prins and Menzel, 1994). The algorithm uses visible, 3.9, 10.7 and 12 micron data. The Multi-angle Imaging SpectroRadiometer (MISR) that flies aboard the NASA TERRA satellite has also been used to detect fire plumes (Kahn et al., 2007).

Lidars are often the sensor of choice for measuring aerosols properties. The distance to which these sensors can make measurement varies depending on their transmitted power and aerosol density. Ground based systems have reported ranges of 10-20 km and heights of 4-10 km (Banta et al. 1992, Colarco et al. 2004, Müller et al. 2005, WindTracer 2008). Smoke aerosol detection is carried out from the Cloud-Aerosol Lidar with Orthogonal Polarization (CALIOP) that flies aboard the CALIPSO satellite (Labonne et al., 2007). Fire detection in visible satellite images is impaired if thick clouds are present between the satellite and the monitored area.

Detection of smoke from satellite is generally done by subjective identification of plumes from visible imagery such as that from GOES. However, automated techniques based on estimated optical depth have been developed for GOES (e.g., Zeng, et al., 2008).

Valery.Melnikov@noaa.gov

Interpretation of smoke plumes becomes difficult in the presence of even an intermittent cloud cover. Differences in radiative temperature between the 8, 11 and 12 micron bands have been used to identify dust in the atmosphere (Ackerman, 1997). This technique may provide some information on the location of smoke plumes during both day and night. The MODIS instrument aboard the NASA AQUA and TERRA satellites provide estimates of aerosol optical depth from multi-spectral observations but are only available once daily.

The WSR-88D radars (10 cm wavelength) in the US national network are sensitive enough to detect plumes of wild fires (e.g., Doviak and Zrnic, 1993, section 11.9; Hufford et al. 1998). We present herein radar observations from one of the operational WSR-88D radars and the proof-of-concept polarimetric WSR-88D and discuss new opportunities in plume detection using radar polarimetric parameters.

2. The WSR-88D radar and satellite observations

Several wild fires in Oklahoma could be identified on 12 March 2008 from areas of very high brightness temperatures (dark spots in Fig. 1) in the GOES-12 3.9 micron imagery. Color images of radar reflectivity from the WSR-88D KTLX radar are superimposed on black and white images of 3.9 micron brightness temperature to provide comparisons of the plumes from the fire locations. The first fires determined with GOES-12 appear at 1835 UTC (40 and 100 km south of the radar and marked with red numbers 1 and 2 to the left of dark spots). By 1845, another fire (110 km south southwest from the radar, spot #3) appears before a plume is clearly visible in the radar data. By 2130 UTC, four fires with plumes are visible (spots #2, 3, 4, and 5). Plume #5 is observed at distances 180 km from the radar. In

addition, at least two other fires (spots #6 and 7) are evident in the satellite data but do not have detectable plumes in the radar data.

The plumes are usually seen at the few lowest elevations of the radar antenna scan, from which the vertical extend of the plumes can be estimated. Radar reflectivity fields in fair weather frequently appear uniform up to a certain range and are caused by insects, birds, fluctuations of refractive index and residues of filtered ground clutter. The plume's reflectivity factor can exceed the reflectivity factor of fair weather by 8 to 15 dB. Closer to the radar (downwind from the sources) the plume's echoes merge with clear air echoes; contrast between them diminishes and then disappears. Reflectivity fields of the plumes show directions of smoke displacement and can be used to obtain the areas affected by plumes and to estimate the effectiveness of fire operations.

The origins of the plumes appear to be displaced on the order of 10 km to the north or northeast of the satellite hot spots. This may be due to advection of the smoke by boundary layer winds before the plume ascents high enough to be detected by the radar beam. For example, given an ascent rate of approximately 1/10 of the horizontal wind speed, the plume would be displaced 10 km when reaching 1 km altitude.

3. Polarimetric radar observations

All WSR-88Ds are single polarization radars transmitting and receiving horizontally polarized waves. The polarimetric WSR-88D, KOUN situated in Norman, OK is the proof-of-concept radar on which upgrades to the US weather radar network are being tested (Saffle et al., 2007). The radar is located 27 km to the South-West from KTLX; it simultaneously transmits and receives horizontally and vertically polarized waves (Zrnic et al., 2006). The amplitudes of the transmitted and received waves will be denoted as E_h, E_v and E_{hr}, E_{vr}. Signal paths in the two radar channels are different so the transmitted and received waves acquire hardware phase difference ψ_t and ψ_r. Atmospheric scatterers shift the waves by the differential phase φ_{dp} due to propagastion and scattering so that the measured phase shift is $\psi_t + \psi_r + \varphi_{dp} = \psi_{sys} + \varphi_{dp}$, where $\psi_{sys} = \psi_t + \psi_r$ is usually called the system differential phase. To measure φ_{dp}, the system differential phase should be subtracted from the total phase. On KOUN the phases were $\psi_t = 78^o \pm 2^o$ and $\psi_{sys} = 38^o \pm 1^o$ in March 2008; the intervals show the measurement uncertainties.

We consider herein horizontal sounding which is a good approximation for elevation angles lower than 10^o. Transmittion of polarized radio-waves, their scattering by particles, and reception of the scattered waves can be described by the following matrix equation:

$$\begin{pmatrix} E_{hr} \\ E_{vr} \end{pmatrix} = \begin{pmatrix} 1 & \\ & e^{i\psi_r} \end{pmatrix} \begin{pmatrix} S_{hh} & S_{hv} \\ S_{hv} & S_{vv} \end{pmatrix} \begin{pmatrix} E_h \\ E_v e^{i\psi_t} \end{pmatrix}, \quad (1)$$

where S_{ij} are the scattering coefficients of the medium. In (1) range dependence and radar constants are omitted without loss of generality because we are interested in polarimetric parameters that do not depend on those. Powers P_h and P_v in the receive channels and the correlation function R_{hv} between received waves are:

$$P_h = <|E_{hr}|^2>, \qquad P_v = <|E_{vr}|^2>,$$
$$R_{hv} = <E_{hr}^* E_{vr}>, \quad (2)$$

where the brackets stand for ensemble averaging and the asterisk denotes complex conjugate. From (2), differential reflectivity Z_{DR}, the differential phase shift φ_{dp} and copolar correlation coefficient ρ_{hv} are obtained

$$Z_{DR} = 10 \log Z_{dr}, \qquad Z_{dr} = \frac{P_h}{P_v}, \quad (3a)$$

$$\rho_{hv} = \frac{|R_{hv}|}{(P_h P_v)^{1/2}}, \qquad \psi_{dp} = \arg(R_{hv}), \quad (3b)$$
$$\varphi_{dp} = \psi_{dp} - \psi_{sys}$$

On the KOUN, six radar parameters are measured from each range location. These are reflectivity (Z), Doppler velocity, Doppler spectrum width, Z_{DR}, ψ_{dp}, and ρ_{hv}.
In Fig. 2, fields of the polarimetric parameters are presented for 2245 UTC, March 12th, 2008. The three plume echoes, i.e. fires #2, 3, and 4 discussed above are clearly seen. To mitigate noise influence on the polarimetric parameters, Z_{DR} and ρ_{hv} were estimated using the 1-lag correlation functions described by Melnikov and Zrnic (2007).

Differential reflectivity in the plumes is large and positive indicating presence of non spherical and horizontally oriented plume particles. The copolar correlation coefficient field shows that the plumes have very low ρ_{hv} and can be easily distinguished from clear air returns. Such low ρ_{hv} suggests that these plumes contain highly non spherical particles. Small values of ρ_{hv} cause significant increase in the variance of differential reflectivity and differential phase, hence the fields of φ_{dp} and Z_{DR} appear noisy in the region of the plume echo. Jones and Christopher (2008) reported on low ρ_{hv} in a major apartment fire smoke observed with 5-cm wavelength radar.

The sky at the time of radar observations was cloudy as seen in Fig. 3. The picture of the sky in the left panel was taken in the South direction from the KOUN location and the visible satellite image is in the right panel. The clouds made identifications of plumes from satellites very difficult, almost impossible without radar data.

Fig. 4 clearly demonstrates the difference in the polarimetric parameters of the plumes, clouds, and clear air returns. The figure is a vertical cross section collected with antenna moving vertically from 0 to 60°. It is seen that KOUN observes the clouds to distances about 35 km. The plume is located at ranges from about 40 to 75 km. The presence of clouds allows simultaneous analysis of polarimetric properties of clouds and smoke plumes. Radar signals from clouds and smoke are weak; to eliminate noise influence on polarimetric variables, the correlation estimators were used (Melnikov and Zrnic, 2007). Fig. 5 depicts distributions of ρ_{hv}, ψ_{dp}, and Z_{DR} in smoke plumes and clouds. The smoke's ψ_{dp} distribution is shown in Fig. 5(a) with the thin line and its smoothed 21-point distribution is shown with the thick solid line. It is seen from Fig. 5 that the clouds' distributions are much narrower than the plumes' ones which is a result of low ρ_{hv} in smoke. The most frequent values of ψ_{dp} are 38° and 26° in the clouds and smoke; therefore φ_{dp} = 26 ° – 38 ° = -12°±2° in smoke because ψ_{sys} = 38°±1°. The mean Z_{DR} are 2.8 and 0.6 dB and the mean ρ_{hv} are 0.41 and 0.98 in smoke and clouds with measurement uncertainties of ±0.1dB and ±0.1. These uncertainties have been obtained with the analysis by Zrnic et al. (2006) and Melnikov and Zrnic (2007). In the next section we design a model that explains these measured values.

3. *The model*

Little is known about particles in smoke plumes that scatter centimeter wavelength radiation. Information obtained from light scattering cannot be directly applied to cm-wavelength radiation; radar can sense small amount of large particles, i.e., the far end of the size distribution that has little effect on optical properties. For instance Rogers and Brown (1977) reported on significant radar signals at 3-cm radiation at vertical sounding of smoke and no signal from optical ceilometer. Shapes of these particles are unknown. Analyzing 3-cm radar data from forest fire smoke Banta et al. (1992) came to a conclusion that scatterers are needle-like most probably. From strong positive differential reflectivities in plumes (Fig. 5b) we can conclude that the scatterers are quite non-spherical and tend to be oriented horizontally. Non uniformities of the wind destroy horizontal orientation of the particles so that they can be characterized by an angle distribution across horizontal plane.

Dielectric properties of ash particles at centimeter wavelengths are unknown also. Cempbell et al. (1969) and Adams et al. (1996) measured the dielectric permittivity ε of volcanic ashes at radar wavelengths in interval 2.8-0.03i to 20-3.4i but those ashes consisted of rock substances whereas biomass burning ashes have organic origin. Large ash particles in smoke plumes could contain water (ε = 80-25i) in their not completely burned cores that introduces more uncertainty into their dielectric properties. The real part of ε provides the main contribution to backscattered waves and we consider it in interval 3 to 80.

Geometry of the particles and incident waves are sketched in Fig. 6. The propagation direction of the radio waves is determined by vector $\vec{k}$ that lies along the x-axis. Consider reflection by spheroidal particles with three principal dimensions a, b, and c and the axis of rotation OO'. For oblate plate-like scatterers, $b < a = c$ and for prolate needle-like particles, $b > a = c$. Orientation of the particle is characterized by two Euler's angles θ and φ. The matrix coefficients for n-th scatterer in (1) are

$$S_{hh}^{(n)} = \alpha_a + \Delta\alpha \sin^2\theta \ \sin^2\varphi\,, \qquad (4a)$$

$$S_{hv}^{(n)} = \Delta\alpha \ \sin\theta \ \cos\theta \ \sin\varphi\,, \qquad (4b)$$

$$S_{vv}^{(n)} = \alpha_a + \Delta\alpha \ \cos^2\theta \ , \qquad (4c)$$

$$\Delta\alpha = \alpha_b - \alpha_a\,,$$

Where α_a and α_b are polarizabilities along *a* and *b*. To get S_{ij} in (1), we have to sum up (4) for all scatterers in the radar volume. Zrnic and Ryzhkov (2004) calculating intrinsic polarimetric parameters of chaff (prolate scatters) used a similar approach but herein we consider simultaneous incidence of horizontally and vertically polarized waves.

At S-band, the smoke particles can be considered as Rayleigh scatterers and the polarizabilities for oblate and prolate scatterers can be found in e.g., Bohren and Huffman 1983, section 5.3. To perform averaging in θ for oblate particles, we consider uniform distribution in θ from 0 to some θ_o, which will be referred to as maximal "flutter" angle and is a model parameter.

Measured polarimetric parameters (3) depend on the mean aspect ratio *b*/*a* which is another parameter of the model. So we have four unknown parameters: *b*/*a*, θ_o, ε, and the shape, i.e., oblate or prolate particles, and try to obtain them from three measured values: Z_{DR}, φ_{dp}, and ρ_{hv}. The latter parameters are measured with accuracies exposed in the previous section, i.e., ±0.1 dB, ±2°, and ±0.1. So we try to map *b*/*a*, θ_o, and ε to the measured polarimetric parameters in the following intervals

$$2.7 \le Z_{DR} \le 2.9 \text{ dB}, \quad -14 \le \varphi_{dp} \le -10^o, \quad 0.40 \le \rho_{hv} \le 0.42 \qquad (5)$$

for oblate and prolate scatterers separately. Three parameters *a*/*b*, θ_o, and ε that satisfy (5) can be represented with a three dimensional graph as shown in Fig 7. The existence of solutions for prolate and oblate scatters indicates that both types of scatterers can satisfy (5); but the plate-like scatterers have to have aspect ratios larger than 40. For oblate scatterers this ratio is significantly loose: *b*/*a* > 4 with the median about 7. The maximal flatter angles span narrow intervals for both type of scatterers with the medians near 53° (needles) and 66° (plates).

The dielectric constants for the needles has to be larger than 10 whereas for the plates, ε > 35. The latter can occur probably if the plates have cores containing water. Analyzing cross-polarization 3-cm wavelength radar data from forest fire, Banta et al. (1992) concluded that the scatterers are needles most likely; nevertheless they did not exclude plates as well.

To narrow uncertainty in deducing *a*/*b* and ε, a technical prospect can be employed. Z_{DR} does not depend on phase shift ψ_t but φ_{dp} and ρ_{hv} do. Existing KOUN's hardware does not allow changing ψ_t but in the near future the radar (after acquiring the polarimetric capability planed for the WSR-88Ds) will be able to change the phase of transmitter radiation. This will allow obtaining R_{hv} at different ψ_t. R_{hv} is very sensitive to ψ_t. This is demonstrated in Fig. 8 for ε = 5 and 30 and θ_o = 53° for needle-like scatterers. It is seen from Figs 8(a, c) that ρ_{hv} strongly depends on ψ_t for *a*/*b* < 0.5. The differential phase changes sign at ψ_t = 90° (Fig. 8 b,d) and can be measured at ε > 4. Dependencies in Fig. 8 do not change much in interval of θ_o from 40° to 60°. So by measuring φ_{dp} and ρ_{hv} at different ψ_t, parameters *a*/*b* and ε can be obtained with fine accuracy. It will allow measuring the properties of large smoke particles remotely.

4. *Conclusions*

Radar observations of smoke plumes can be used to detect fire smoke at distances within about 180 km, monitor smoke drift, and estimate air quality. Cloudiness makes recognition of smoke plumes from the satellites difficult but does not affect radar observations. Low correlation coefficient ρ_{hv} and non zero differential phase φ_{dp} of signals in the horizontal and vertical radar channels indicate smoke. This should be used in smoke recognition among echoes from clouds, precipitation, clear air, insects, and birds.

We described a model that connects measured ρ_{hv}, φ_{dp} and differential reflectivity Z_{DR} with the mean ratio of the minor and major dimensions *a*/*b* of the scatterers, their dielectric permittivity ε, and an angle of flattering θ that is considered to be uniform to some maximum angle θ_o. We considered prolate needle-like and oblate plate-like scatterers and concluded that large smoke particles can be needles with the median *a*/*b* of 7 or plates with *a*/*b* > 40. The maximal flatter angle θ_o is 53°±3° for the needles and 66°±3° for the plates. There could be also a mixture of these types of particles in smoke.

To make more accurate measurements of smoke particles' properties, a strong dependence of φ_{dp} and ρ_{hv} upon transmit differential phase ψ_t can be utilized. Measuring Z_{DR}, ρ_{hv}, and φ_{dp} at different ψ_t, particles' parameters a/b, ε, and θ_o can be determined more precisely. A new polarimetric WSR-88D which will be installed on KOUN will have a capability to change ψ_t.

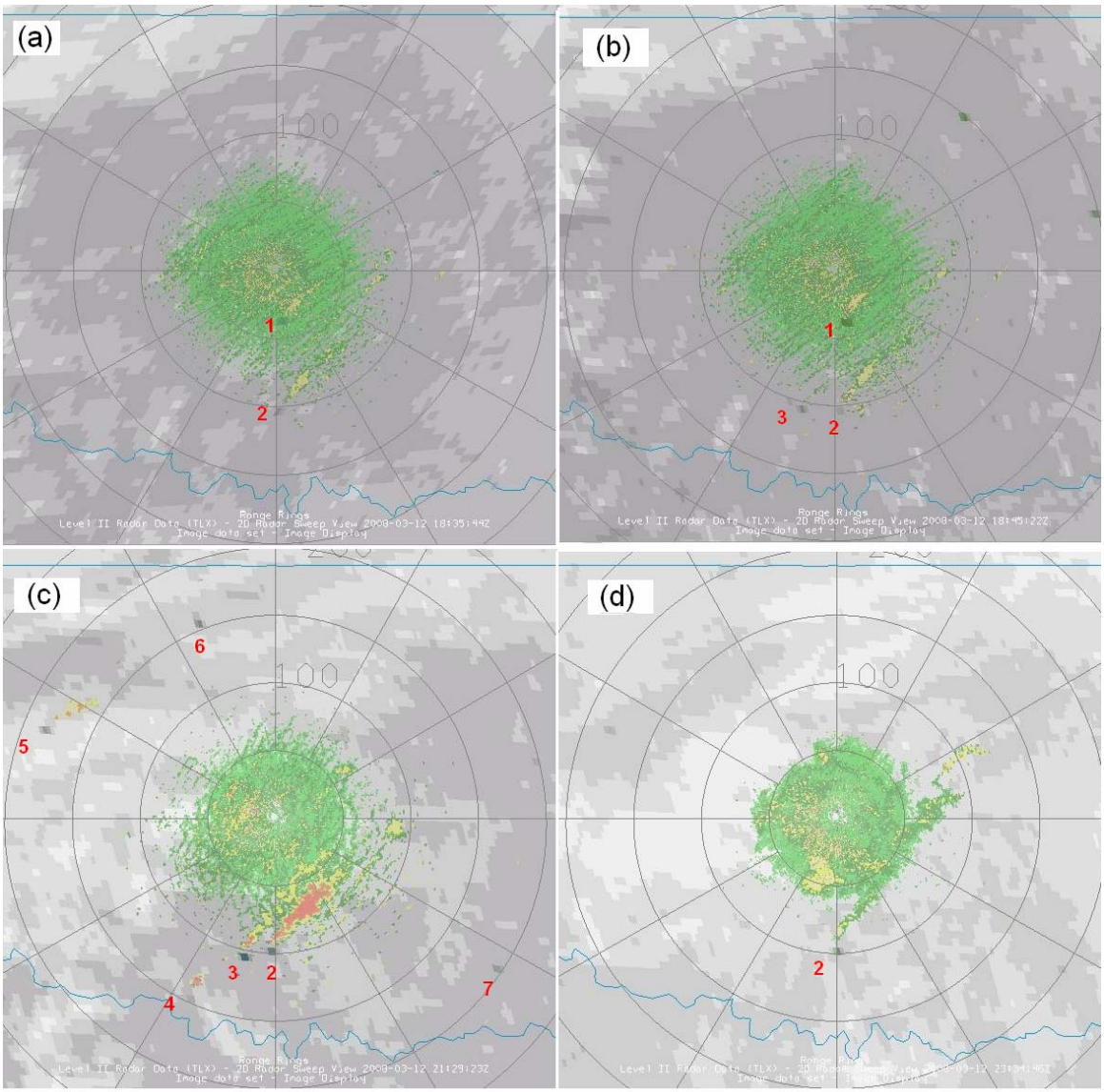

Fig. 1. Radar reflectivity from WSR-88D KTLX superimposed on GOES-12 3.9 micron brightness temperature image. Wild fires from GOES-12 are associated with high brightness temperature (darkest spots). 12 March 2008, (a): 1835, (b): 1845, (c): 2129, and (d) 2334 UTC.

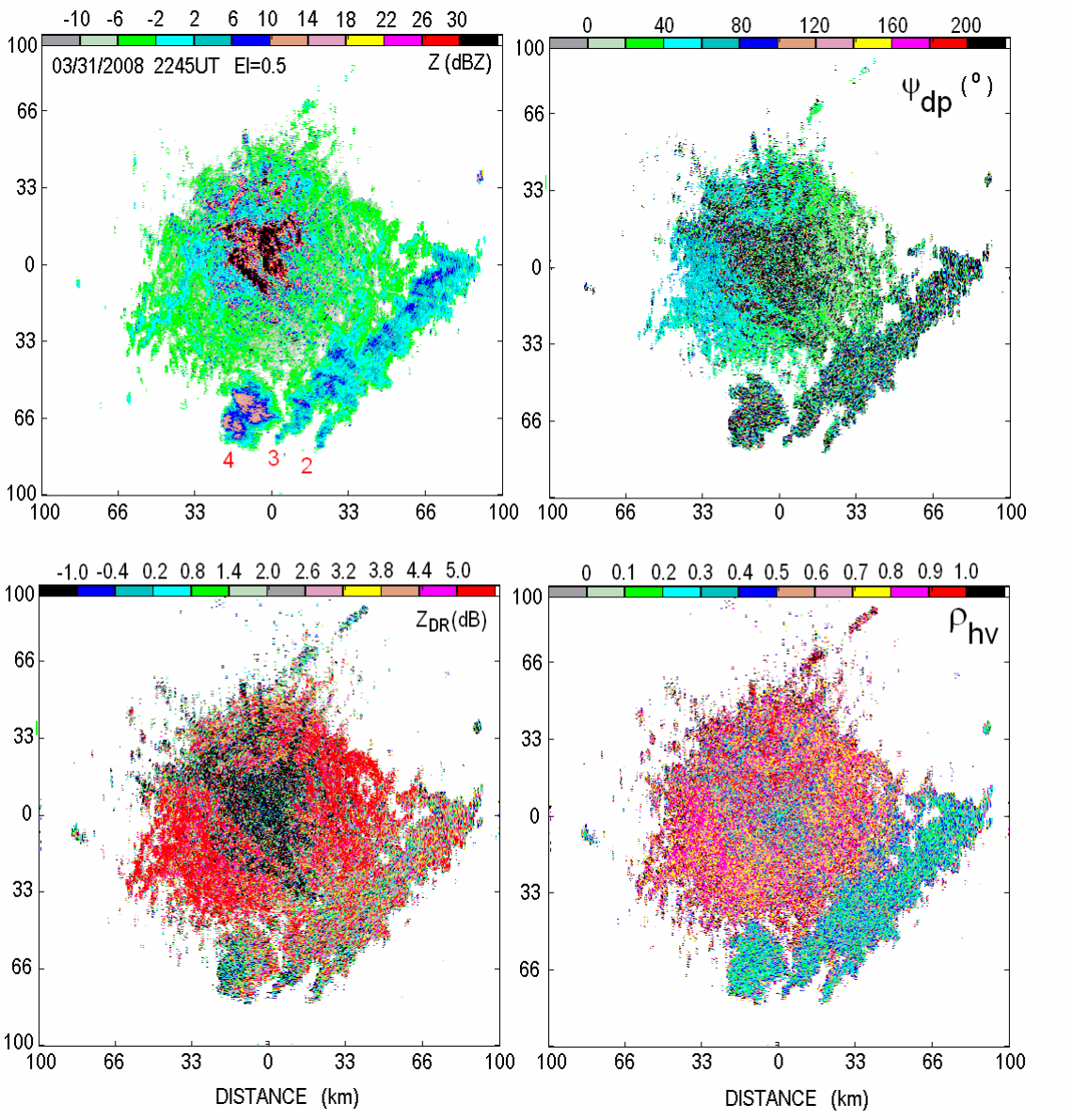

Fig. 2. Fields of reflectivity and polarimetric variables obtained with the WSR-88D, KOUN at 2245 UTC on March 12th, 2008. Antenna elevation is 0.5^{o}.

Fig. 3. (left) Picture of the sky taken at 2250 in the south direction from KOUN. (right): visible satellite image at 2245 for Oklahoma on March 12th, 2008.

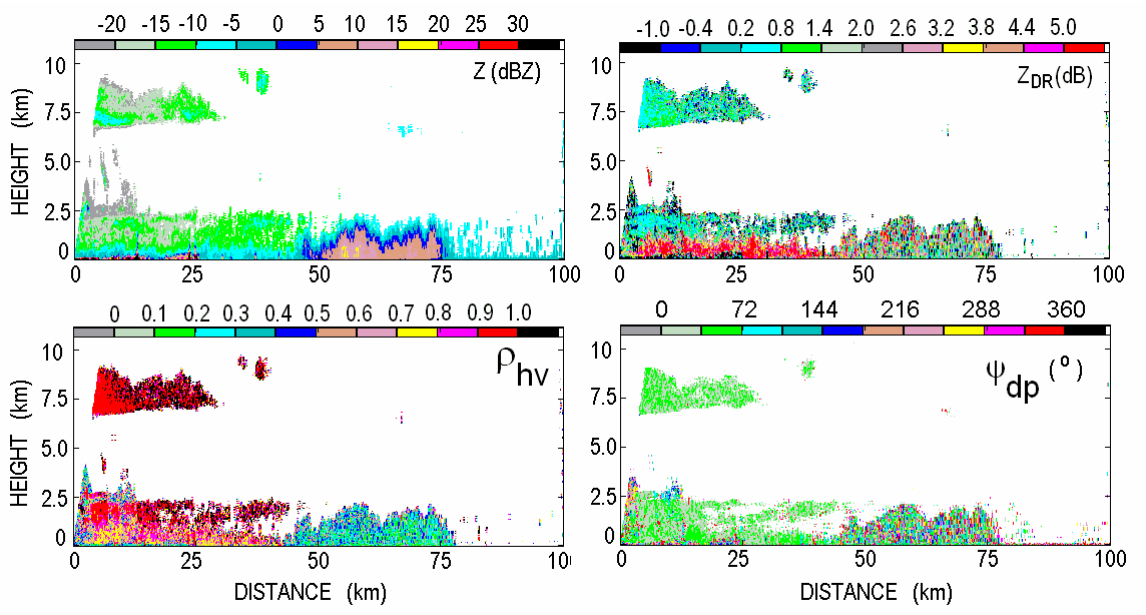

Fig. 4. Vertical cross sections collected with KOUN at 2250 at azimuth 191°. March 12th, 2008.

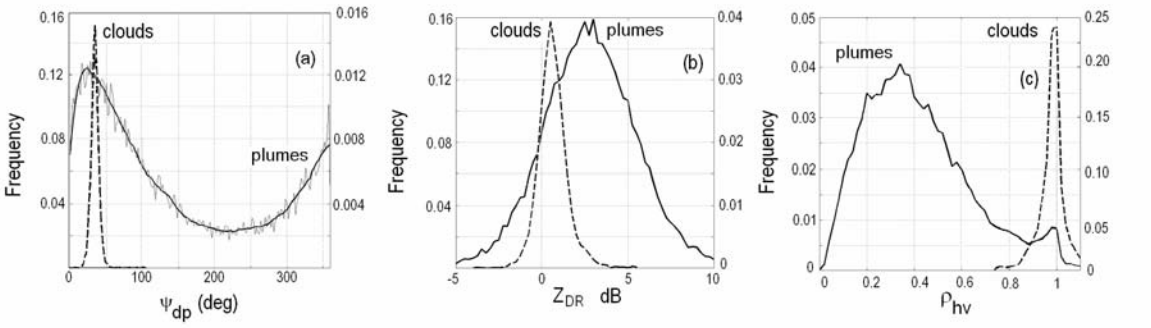

Fig. 5. Distributions of the (a) differential phase ψ_{dp}, (b) differential reflectivity Z_{DR}, and (c) correlation coefficient ρ_{hv} in smoke plumes (solid lines) and clouds (dashed lines) on 12 March, 2008. WSR-88D KOUN. The higher frequency scales in the panels are for clouds and the lower ones are for smoke plumes.

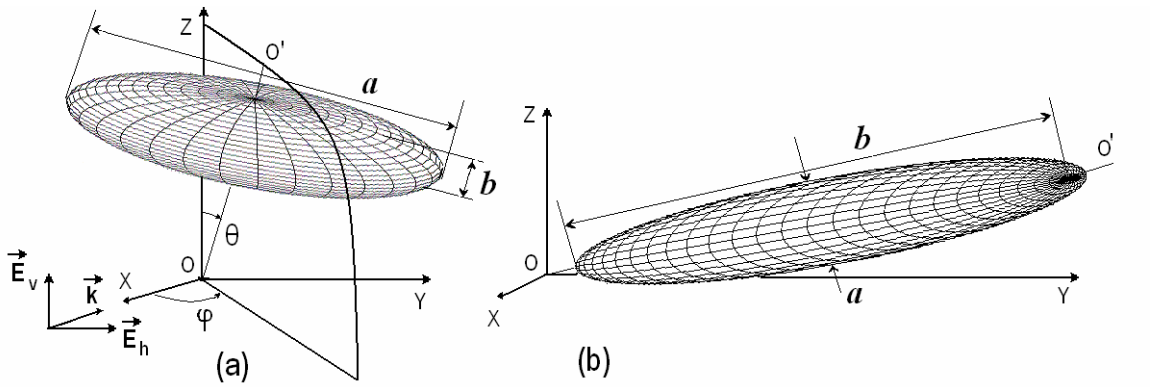

Fig. 6. Oblate (a) and prolate (b) spheroidal scatterers and the incident waves.

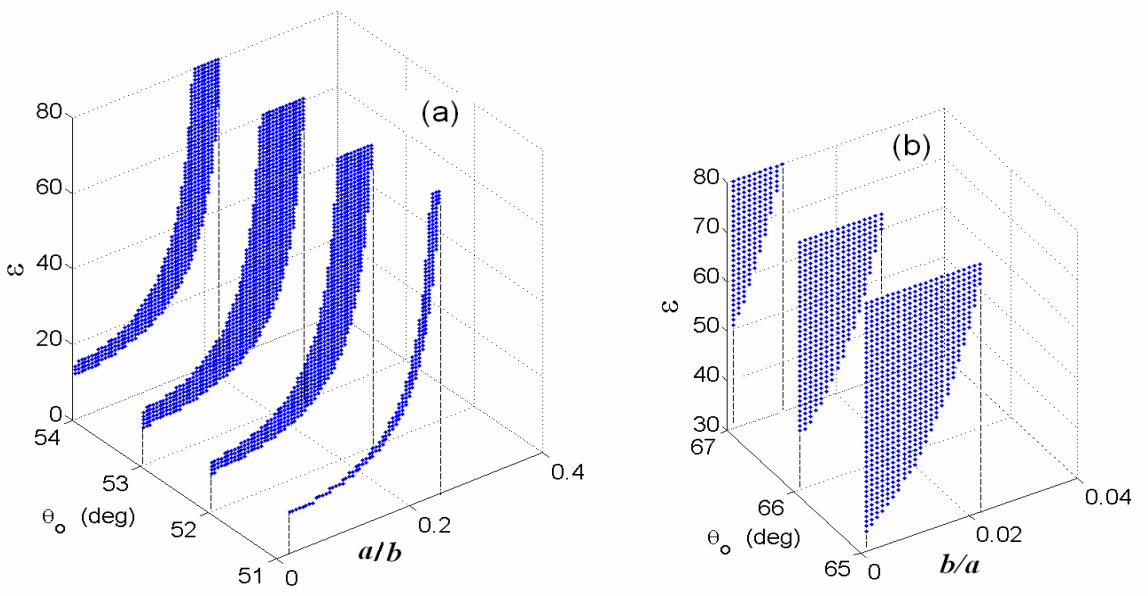

Fig. 7. Cross-section of the 3-dimensional space of b/a, θ_o, and ε that satisfy (8) for (a) prolate and (b) oblate spheroids.

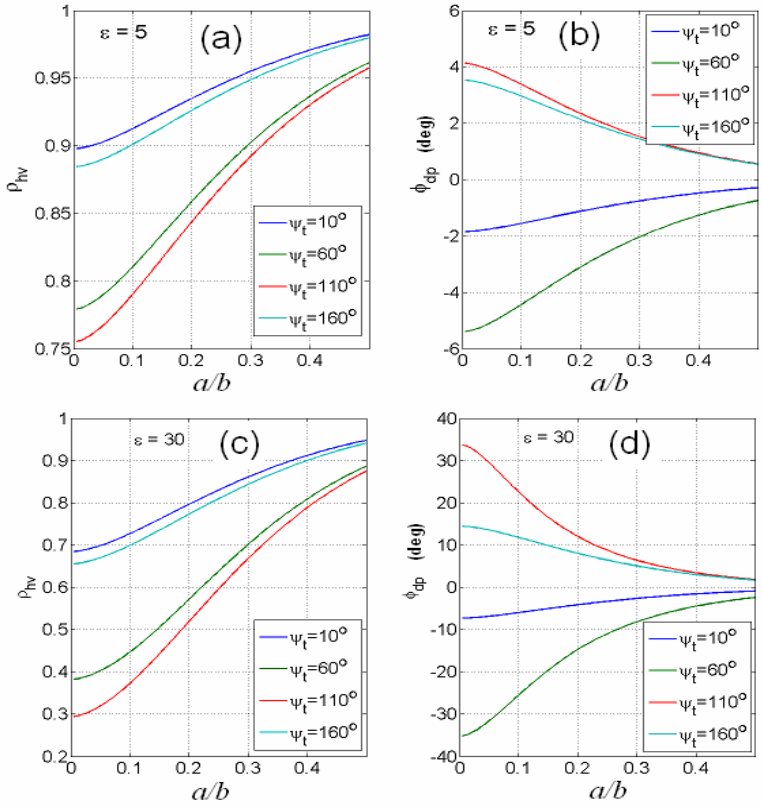

Fig. 8. Dependencies of ρ_{hv} and φ_{dp} on a/b and ψ_t for (a, b) $\varepsilon = 5$ and (c, d) $\varepsilon = 30$ for prolate spheroids at $\theta_{o=} 53^o$.

References

Ackerman, S. A. (1997), Remote sensing aerosols using satellite infrared observations. *J. Geophys. Res.*, **102**, 17069-17079.

Adams, R.J., W.F. Perger, W.I. Rose, and A. Kostinski, 1996: Measurements of the complex dielectric constant of volcanic ash from 4 to 19 GHz. *J. Geophys. Res*., **101**, B4, 8175-8185.

Banta, R.M., L.D. Oliver, E.T. Holloway, R.A. Kropfli, B.W. Bartram, R.E. Cupp, and M.J. Post. (1992), Smoke-Column observations from two forest fires using Doppler lidar and Doppler radar. *J. Applied Meteorol*., **31**, 1328-1349.

Bohren, C.F., and D.R. Haffman, 1983. *Absorption and Scattering of Light by Small Particles,*John Whilley and Son, San Diago, CA.

Cempbell, M.J., and J. Ulrichs, 1969: Electrical properties of rocks and their significance for lunar radar observations. *J. Geophys. Res*., **74**, 5867-5881.

Colarco, P. R., M.R. Schoeberl, B.G. Doddrodge, L.T. Marufu, O. Torres, and E.J. Welton (2004), Transport of smoke from Canadian forest fires to the surface near Washington, D.C. *J. Geophys. Res*., **109**, D06203.

Doviak, R. J. and D. S. Zrnic (1993), *Doppler radar and weather observations*, 2nd ed., Academic Press, 562 pp.

Jones, T.A., and S. A. Christopher, 2008: Variability of Georgia and Florida air quality as a function of radar derived aerosol coverage and height., 15th Joint Conference on the Applications of Air Pollution Meteorology. AMS, New Orleans, LA, J1.3.

Hufford G.L., H. Lee Kelley, and W. Sparkman (1998),Use of real-time multisattelite and radar data to support fire management, *Weather and Forecasting*, **13**, 592-605.

Kahn, R.A., W.H. Li, C. Moroney, D. J. Diner, J.V. Martonchik, and E. Fishbein (2007), Aerosol source plume physical characteristics from space-based multiangle imaging. *J. Geophys. Res*., **112**, D11205, doi:10.1029/206JD007647.

Labonne, M., F._M.Breon, and F. Chevallier (2007), Injection height of biomass burning aerosols as seen from a spaceborne lidar. *Gephys. Res. Lett*. **34**, L11806, doi: 10.1029/2007GL029311.

Melnikov, V.M., and D.S. Zrnic, 2007: Autocorrelation and cross-correlation estimators of polarimetric variables. *J. Atmos. Ocean. Technol*., **24**, 1337-1350.

Melnikov, V.M., D.S. Zrnic, R.M. Rabin, and P.Zhang, 2008: Radar polarimetric signatures of fire plumes in Oklahoma. *Geophys. Res. Lett*., **35**, L14815, doi:10.1029/2008GL034311.

Müller, D., I. Mattis, V.Wandinger, A. Ansmann, D. Althausen, and A. Stohl. (2005), Raman lidar observations of aged Siberian and Canadian forest fire smoke in the free troposphere over Germany in 2003: Microphysical particle characterization. *J. Geophys. Res.*, **110**, D17201.

Prins, E.M., and W.P. Menzel (1994), Trends in South American biomass burning detected with the GOES visible infrared spin scan radiometer atmospheric sounder from 1983 to 1991, *J. Geophys. Res*., **99**, 16719-16735.

Rogers, R.R., and W.O.J. Brown (1977). Radar observation of a major industrial fire. Bull. *Amer. Meteorol. Soc.*, **78**, 803-814.

Saffle, R. E., G. S. Cate, and M. Istok (2007), NEXRAD Product Improvement—Update 2007. *23rd Conf. on IIPS, Amer. Meteorol. Soc*., San Antonio, TX, 5B.1.

Zeng, J., S. Kondragunta, T. Beck (2008), Evalua tion of GOES-12 smoke detection algorithm using OMI aerosol products. AGU 2008 Spring Meeting Abstracts, A2.

Zrnic D.S., and A.V. Ryzhkov (2004), Polarimetric properties of chaff. *J. Atmos. Ocean. Technol*., **21**, 1017-1024.

Zrnic D.S., V. M. Melnikov, and J. K. Carter (2006), Calibrating differential reflectivity on the WSR-88D. *J. Atmos. Ocean. Technol*., **23**, 944-951.